nature electronics

SUPPLEMENTARY INFORMATION

https://doi.org/10.1038/s41928-020-0388-x

In the format provided by the authors and unedited.

Solution-processed upconversion photodetectors based on quantum dots

Wenjia Zhou[1], Yuequn Shang[1], F. Pelayo García de Arquer[2], Kaimin Xu[1], Ruili Wang[1], Shaobo Luo[1], Xiongbin Xiao[1], Xiaoyu Zhou[3], Ruimin Huang[3], Edward H. Sargent[2] and Zhijun Ning[1]✉

[1]School of Physical Science and Technology, ShanghaiTech University, Shanghai, China. [2]Department of Electrical and Computer Engineering, University of Toronto, Toronto, Ontario, Canada. [3]Shanghai Institute of Materia Medica, Chinese Academy of Sciences, Shanghai, China. ✉e-mail: ningzhj@shanghaitech.edu.cn

Solution-processed Upconversion Photodetectors Based on Quantum Dots

Wenjia Zhou[1], Yuequn Shang[1], F. Pelayo García de Arquer[2], Kaimin Xu[1], Ruili Wang[1], Shaobo Luo[1], Xiongbin Xiao[1], Xiaoyu Zhou[3], Ruimin Huang[3], Edward H. Sargent[2], Zhijun Ning[1,*]

[1] School of Physical Science and Technology, ShanghaiTech University, 393 Middle Huaxia Road, Pudong, Shanghai, 201210, China

[2] Department of Electrical and Computer Engineering, University of Toronto, 10 King's College Road, Toronto, Ontario M5S 3G4, Canada

[3] Shanghai Institute of Materia Medica, Chinese Academy of Sciences, 555 Zuchongzhi Road, Shanghai,201203, China

Correspondence and requests for materials should be addressed to Z.N. (Email： ningzhj@shanghaitech.edu.cn)

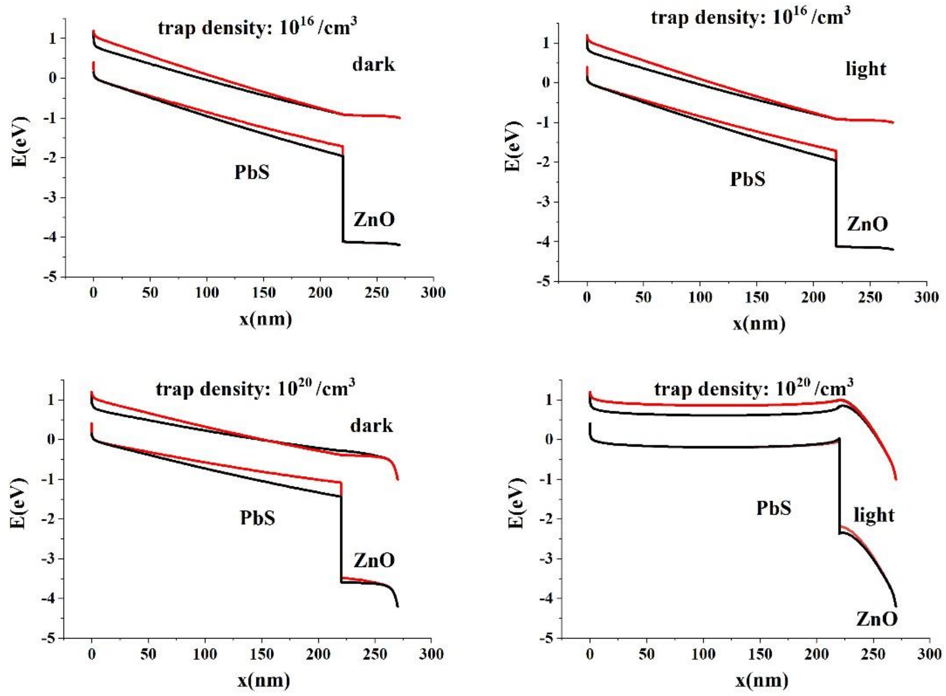

Supplementary Figure 1. SCAPS simulation results for photodetectors using higher mobility ZnO. When electron traps are present, charge accumulation promotes a greater degree of band bending, facilitating hole tunneling from the ITO reservoir. The mobility values for ZnO used here are 0.05, 0.5, 1, 10, and 100 cm^2/Vs.

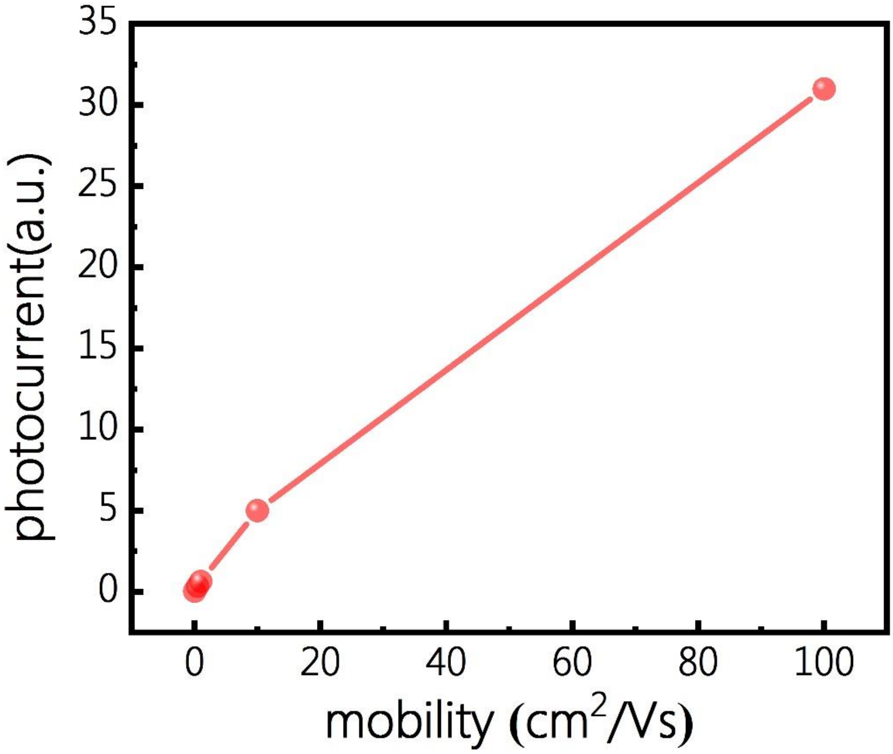

Supplementary Figure 2. SCAPS simulation results for the photodetector photocurrent as a function of the mobility of ZnO.

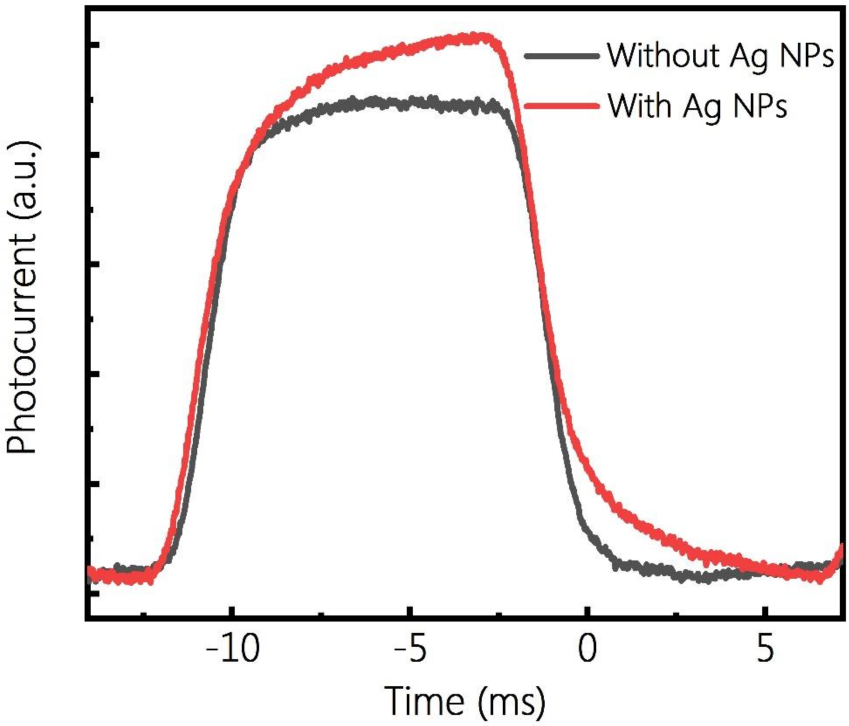

Supplementary Figure 3. Transient photocurrents of the ZnO films without and with Ag nanoparticle.

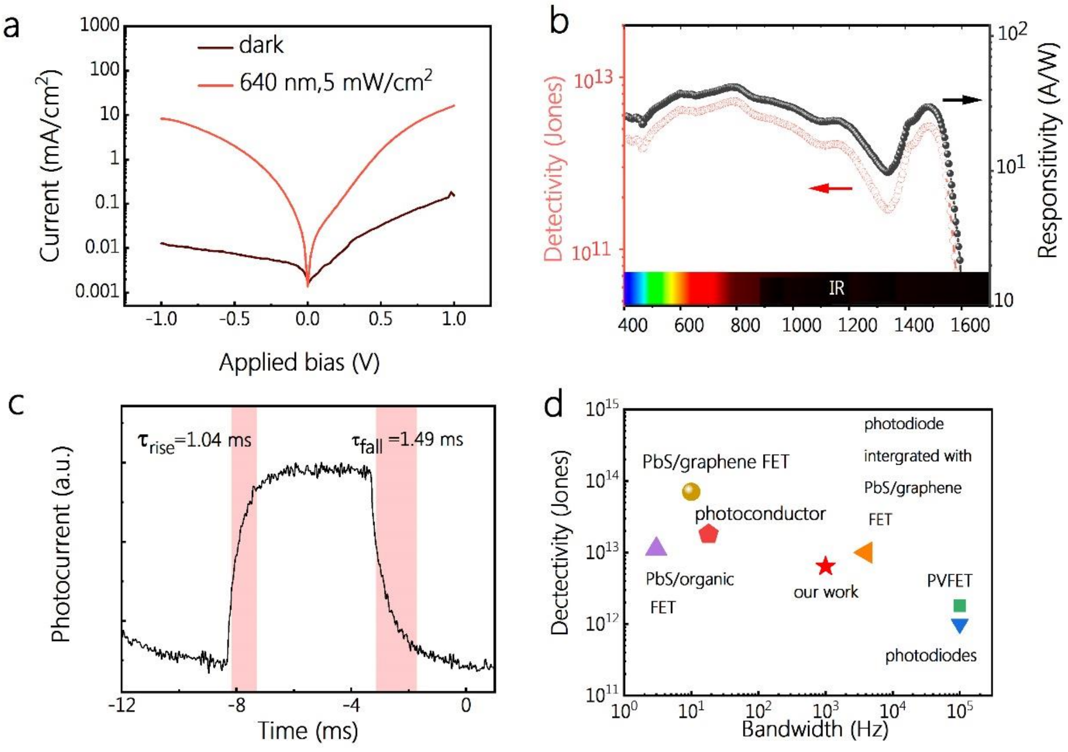

Supplementary Figure 4. Photodetector performance. (a) Dark and light I-V characteristics of the CQD photodetector; illumination is at 640 nm and 5 mW/cm^2. (b) Wavelength dependence of detectivity (D*) and responsivity under -1 V reverse bias at 180 Hz. The maximum light detecting range can go to 1600 nm. (c) Response speed of the photodetector. The device shows a rise time of approximately 1 ms. (d) Detectivity and bandwidth of CQD photodetectors (FET: field effect transistor, PVFET: photovoltage field effect transistor).

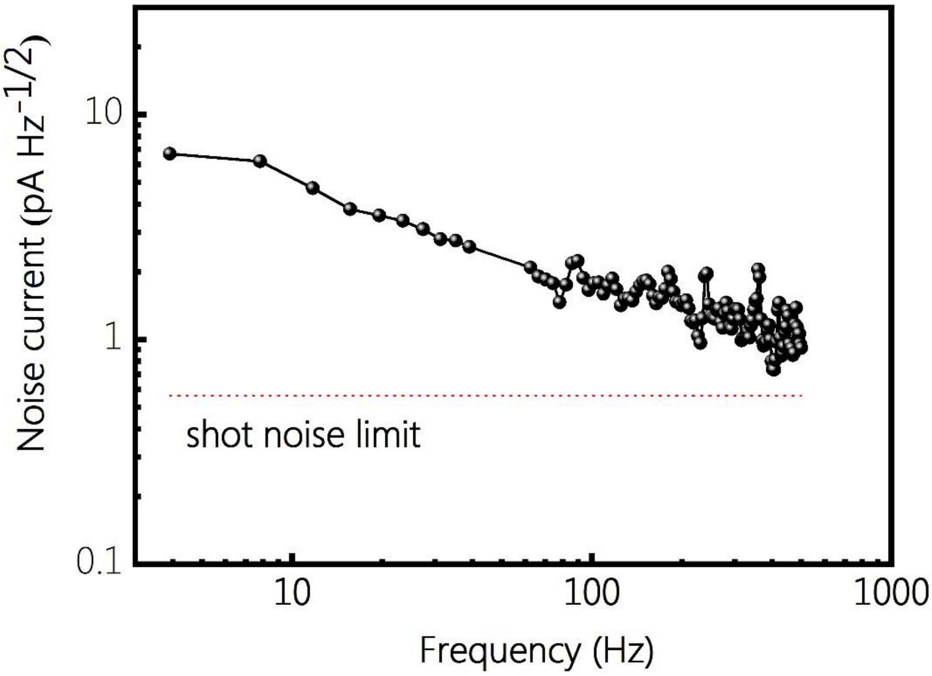

Supplementary Figure 5. Noise spectra of the photodetector part under -1 V bias in the dark environment.

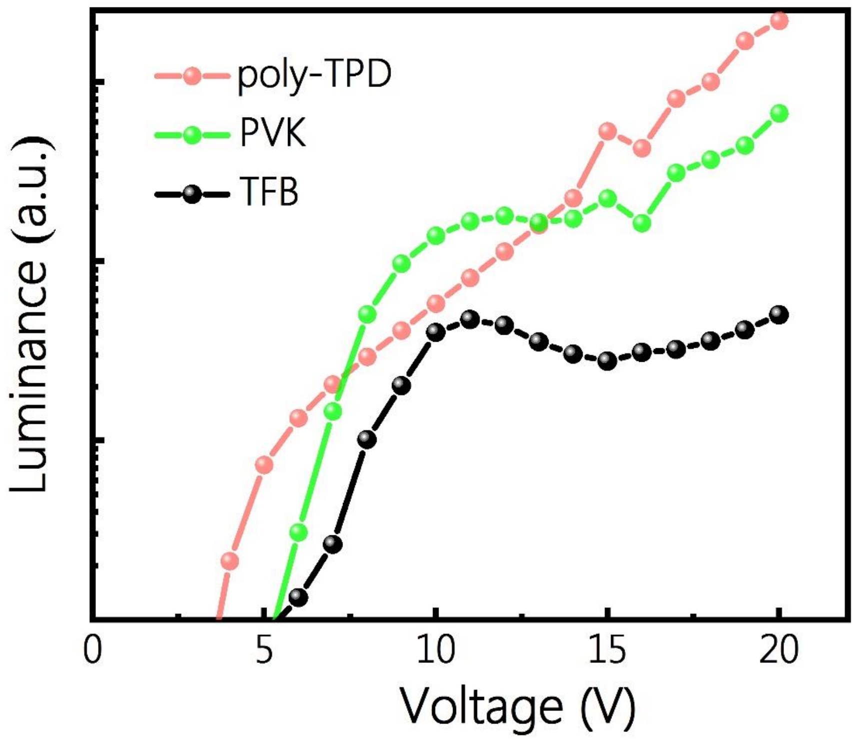

Supplementary Figure 6. Performance of upconversion devices using different hole-transporting layers including poly (9, 9-dioctyl-fluorene-co-N(4-butylphenyl)diphenylamine) (TFB), poly (N-vinylcarbazole) (PVK), and polymeric triphenyldiamine (poly(N,N'-diphenylben - zidine diphenylether) (poly-TPD).

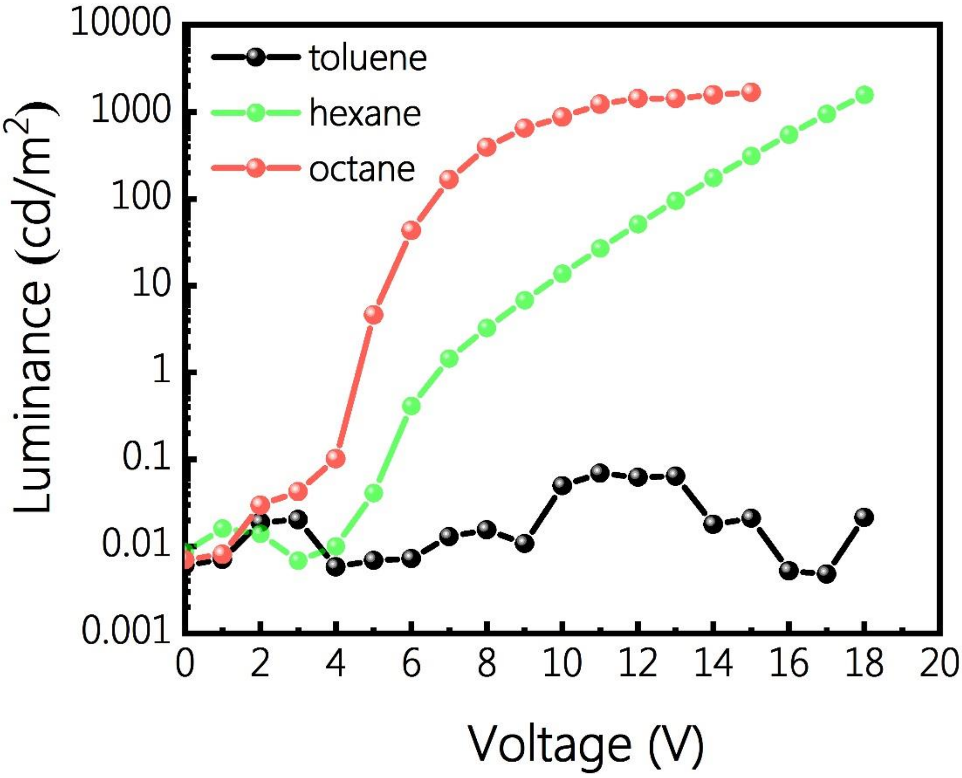

Supplementary Figure 7. Performance of upconversion devices using different solvents for the fabrication of CdSe/ZnS layer.

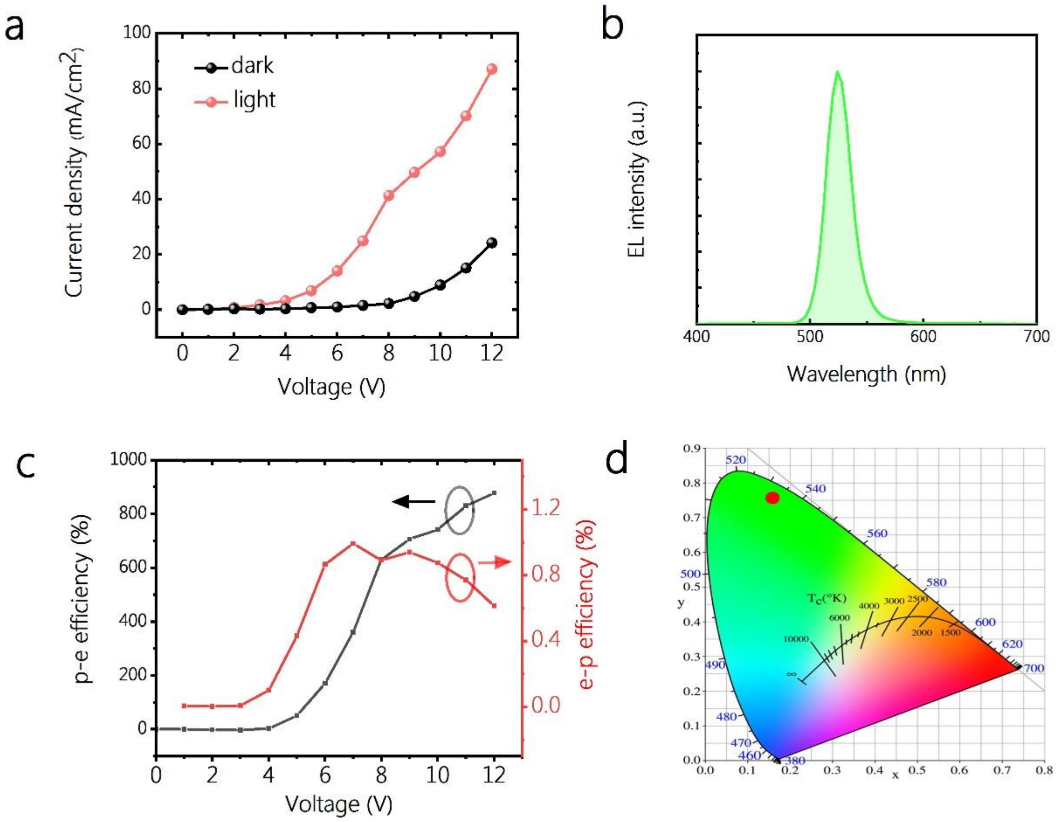

Supplementary Figure 8. Supplementary device performance of the bottom-emitting upconversion devices. (a) I-V characteristics of the device in the dark and light. (b) EL spectrum of the upconversion device. (c) e-to-p efficiency and p-to-e efficiency of the device at different operation voltages. (d) CIE coordinates for the EL spectrum in (b).

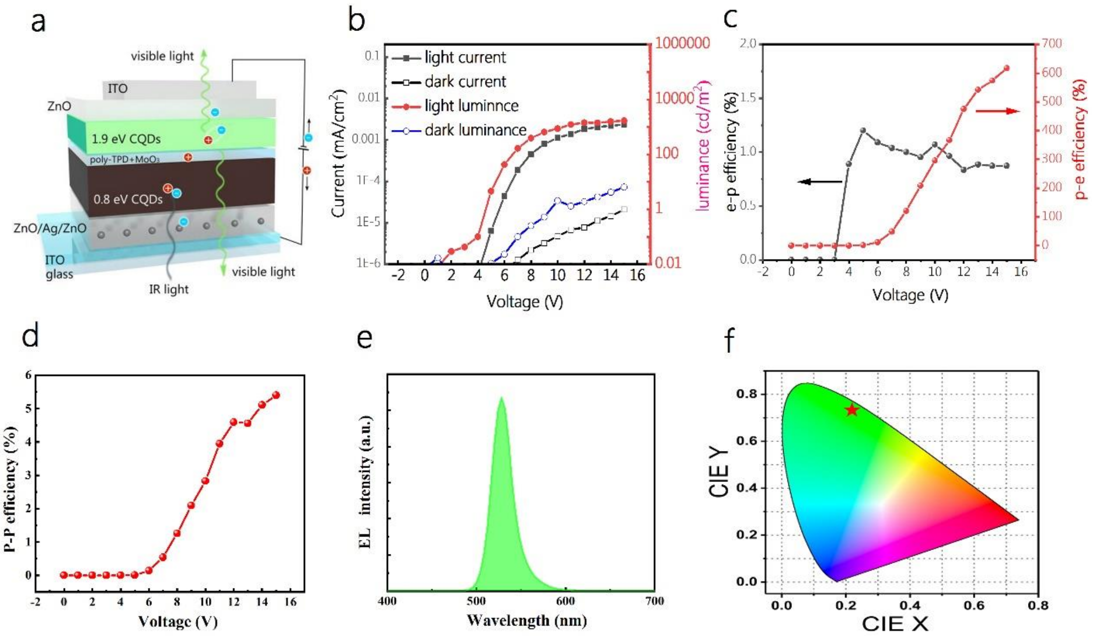

Supplementary Figure 9. Device performance of the upconversion devices using top-emitting structure. (a) Structure of the top emitting upconversion device. (b) Luminance-voltage characteristics and current-voltage characteristics of the device in dark and light condition. (c) e-to-p efficiency and p-to-e efficiency of the device at different operation voltages. (d) Infrared to visible photon-to-photon (p-p) efficiency of the device. (e) EL spectrum of the upconversion device. (f) CIE coordinates for the EL spectra in (e).

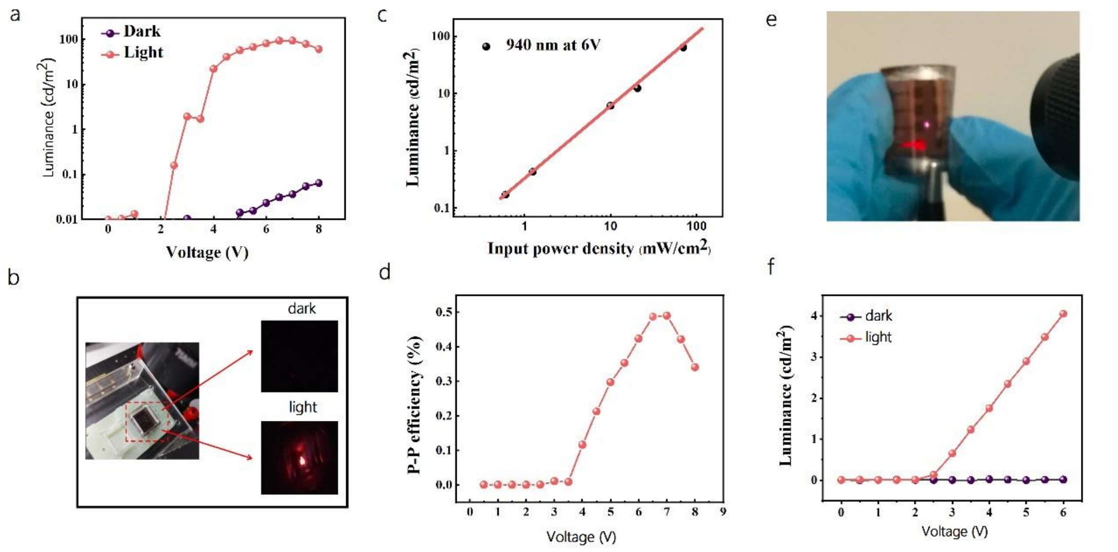

Supplementary Figure 10. Device performance of the upconversion devices using red CQDs. (a) Luminance-voltage characteristics of the device in dark and light condition. (b) Photograph of the sample clamped in the measurement box (left), and images of the device (area of 0.05 cm^2) with and without infrared light (940 nm). (c) Infrared power dependence of the luminance of the upconversion device. Linear increase of current is observed as the increase of illumination intensity. (d) Infrared to visible p-to-p efficiency of the device. (e) Photograph of the flexible device working at a bending state. (f) Luminance-voltage characteristics of the flexible device at a bending state. The turn-on voltage is only 2 V.

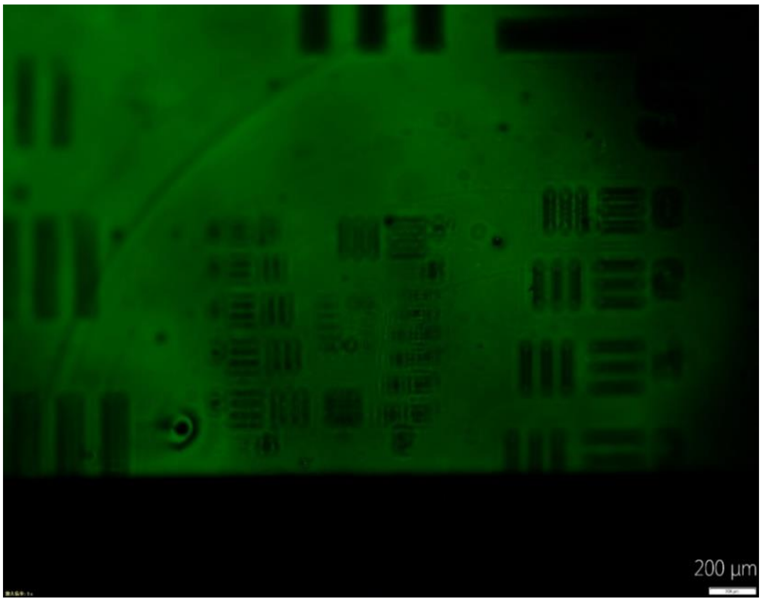

Supplementary Figure 11. Resolution test result using a line pair resolution test target. The spatial resolution exceeds 16 line pair/mm measured by a resolution test target.

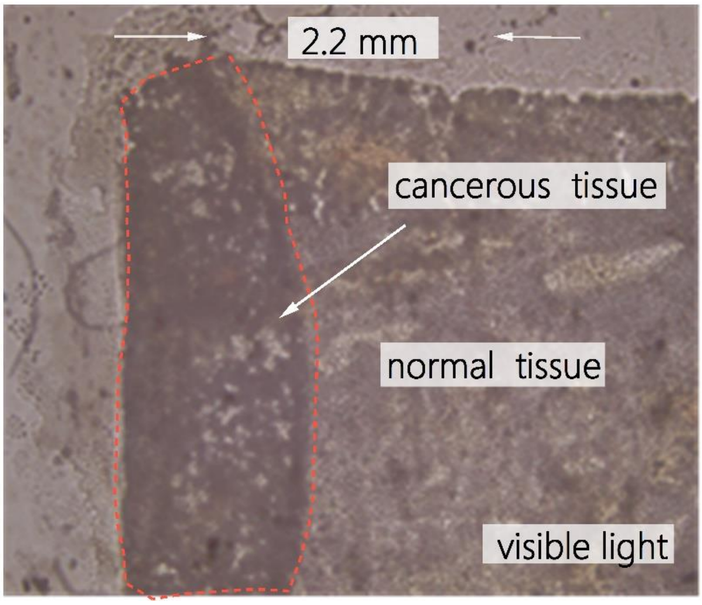

Supplementary Figure 12. Visible photograph of a tissue section (100 μm wide) from a mouse breast cancer smaple under visible light.

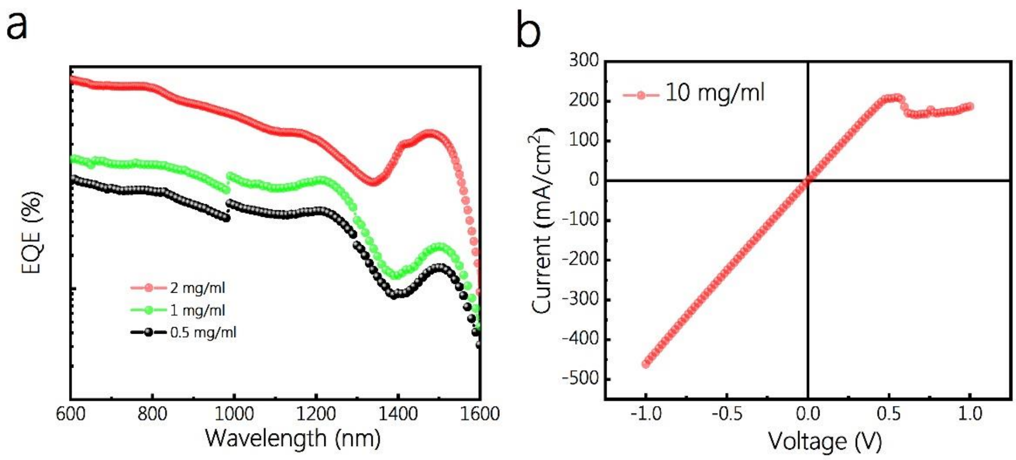

Supplementary Figure 13. Performances of photodetectors using different concentration of Ag nanoparticles. (a) EQE of photodetector using different concentration of Ag nanoparticles. (b) I-V curve of the devices with large concentration of Ag nanoparticles (10 mg/ml).

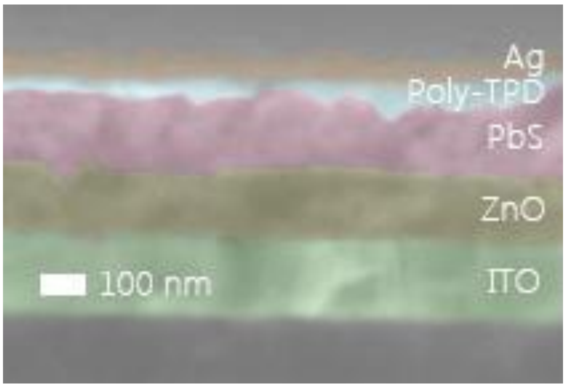

Figure S14. Cross-sectional SEM image of PbS QD photodetector.

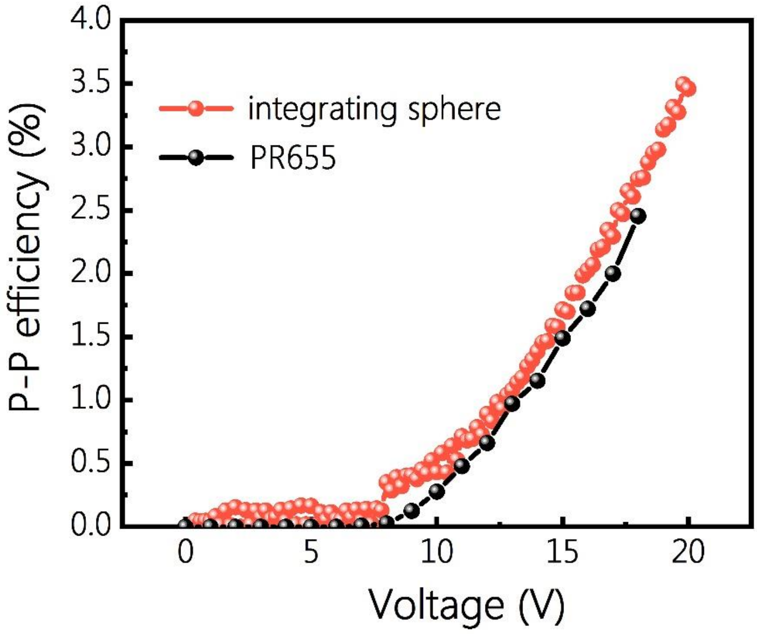

Supplementary Figure 15. Performances of top emitting upconversion devices using different measuring methods.

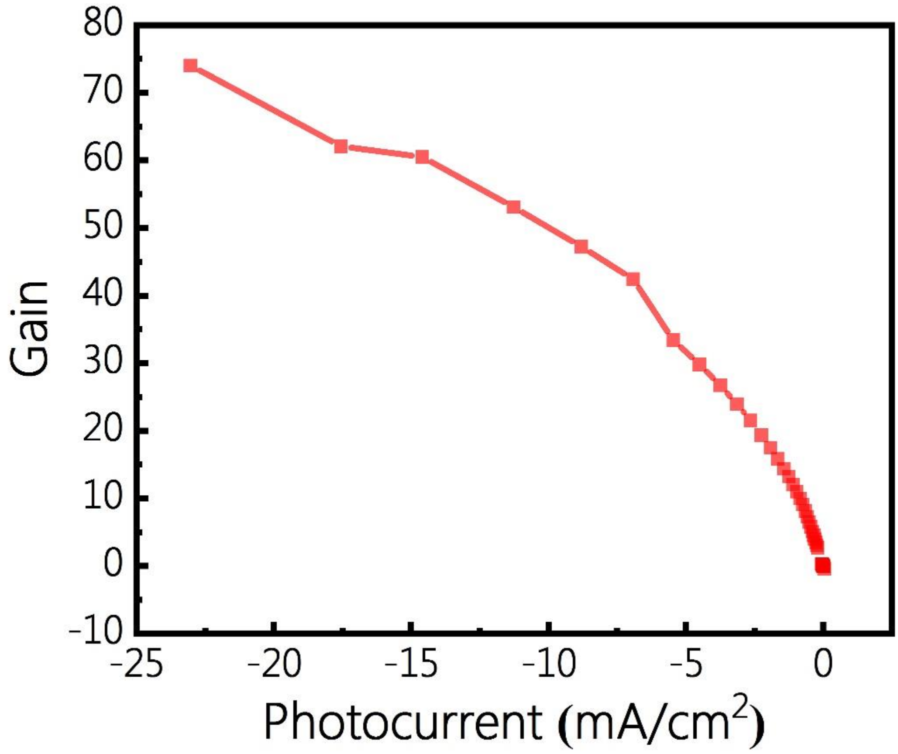

Supplementary Figure 16. EQE vs photocurrent curve of the photodetector only device. We estimate the theoretical limiting of the top- emitting device as follows. Assuming a top LED with an external quantum efficiency of over 10% in the current density range from 10 mA/cm^2 to 200 mA/cm, [1] and a photodetector with a gain of 60 in the operating current range 15 mA/cm^2 to 25 mA/cm^2 (Figure S16), with efficient electronic coupling, the theoretic photon to photon conversion efficiency for the upconversion device is 600%. By engineering the device structure and fabrication process, an EQE of 20% for the LED and a gain of 100 for the photodetector could potentially be be achieved. Consequently, an overall photon to photon efficiency for the upconversion device could in theory reach as high as 2000%.

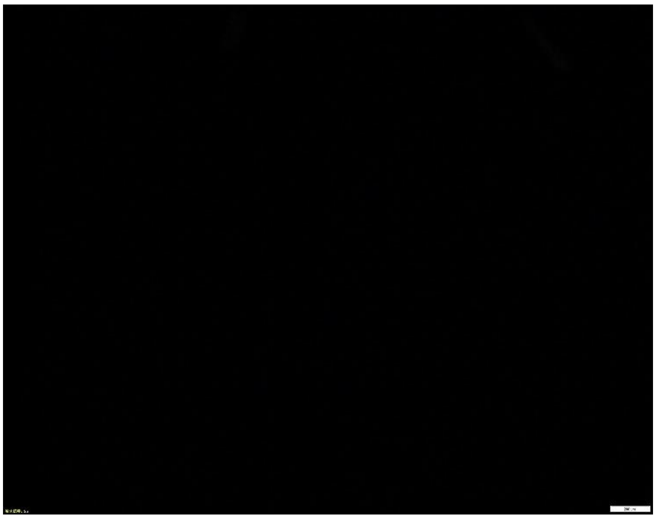

Supplementary Figure 17. Picture of the mask illuminated by 980 nm light directly without upconversion device taken by the CCD. No clear image can be got, which preclude NIR absorption effects in the CCD.

Supplementary Table 1. Details of SCAPS used parameters. The PbS-TBAI layer consists of a parabolic grading combination of the parameters listed and those of PbS-EDT layer (PbS-TBAI l means PbS QDs with TBAI ligands while PbS-EDT means PbS QDs with EDT ligands).

	PbS-EDT layer	**PbS-TBAI layer**	**ZnO layer**
Thickness (nm)	220		120
Bandgap (eV)	0.8	0.8	3.2
Electron affinity (eV)	4.1	4.4	4.2
Permittivity (er)	20	20	66
CB/VB DOS (1/cm^3)	1E19	1E19	1E19
Electron mobility (cm^2/Vs)	0.02	0.02	0.05/0.5/1/10/100 (swept)
N_{donor} (1/cm^3)	0	1E15	1E18
$N_{acceptor}$ (1/cm^3)	1E16	0	0
EDT/TBAI defect (neutral)			ZnO defect (acceptor)
Capture cross section (cm^2)	5E-13	5E-13	
Position below Ec (eV)	0.5	0.5	
Density (cm^{-3})	5E15	5E15	1E16 - 1E20 (swept)

References:

1 Liu, G., Zhou, X. & Chen, S. Very bright and efficient microcavity top-emitting quantum dot light-emitting diodes with Ag electrodes. *ACS Appl. Mater. Interfaces.* **8**, 16768-16775 (2016).